Sociedade Brasileira de Automática (SBA)
XV Simpósio Brasileiro de Automação Inteligente - SBAI 2021, 17 a 20 de outubro de 2021

Handling disturbances with a zone tracking-oriented stabilizing MPC: enlargement of the domain of attraction

Daniel D. Santana * **Márcio A. F. Martins** *

* *Departamento de Engenharia Química, Escola Politécnica, Universidade Federal da Bahia, Rua Aristides Novis, 2, Federação, 40210-630, Salvador, BA, Brazil (e-mail: daniel.diniz@ufba.br, marciomartins@ufba.br)*

Abstract: This work focuses on the hierarchical control structure composed of model predictive control (MPC) and real-time optimization (RTO) layers. Here, a zone tracking-oriented infinite horizon MPC strategy with optimizing targets defined by RTO is proposed. This strategy must comply with eventual unreachable targets and unmeasured disturbances. Consequently, its domain of attraction must be enlarged in order to circumvent infeasibility conditions. This is achieved by imposing terminal equality constraints solely on non-stable states, artificial equilibrium points and softening the bound-type constraints on states with suitable slack variables. Finally, a case study based on an unstable reactor is used to demonstrate the properties of the proposed strategy and the role of the terminal ingredients in the domain of attraction.

Keywords: zone control, enlarged domain of attraction, terminal ingredients, RTO and MPC integration

1. INTRODUCTION

The two-layer hierarchical control schemes are often used to provide plantwide optimization (Scattolini, 2009). In this scheme, an upper layer defines economic targets and pinpoints to the lower layer responsible for tracking them. The former can be designed as an RTO (Real-Time Optimization) based on a rigorous static model of the system. The latter can be an MPC (Model Predictive Control) based on an approximated dynamic model.

The difference between the design of each layer, uncertainties in the system, and unmeasured disturbances can make targets defined by RTO unreachable, which can yield an infeasible solution from the MPC controller (Marchetti et al., 2014). Then, the challenge in the upper layer is to maintain the model updated and tackle uncertainties. One strategy that recently has been used to deal with this issue is to use transient measurements in RTO updates (Krishnamoorthy et al., 2018; Santos et al., 2021). Furthermore, the MPC layer must comply with the desired operating conditions while maintaining both stabilizing properties and the feasibility of the resulting optimization problem, even in the presence of disturbances. Therefore, the challenge here is to enlarge the MPC domain of attraction to tackle infeasible solutions while solving the associated optimization with a lower computational burden in a short time frame.

Another ingredient to provide additional degrees of freedom for the controller is implementing a zone-tracking MPC strategy, in which the output targets are decision variables of the optimization problem (González and Odloak, 2009; Ferramosca et al., 2010). Its integration within the hierarchical control architecture is achieved by imposing RTO evaluated targets on inputs (González and Odloak, 2009; Martins and Odloak, 2016). Furthermore, the stabilizing properties are commonly provided by terminal constraints as an invariant positive set. However, such a task can be tricky for small-scale systems and intractable for large-scale systems. Aiming at the MPC for the tracking case, Ferramosca et al. (2009) included an artificial steady-state mechanism that tracks such targets, in addition to collapsing the terminal set into a terminal equality constraint enforcing all states to be at this steady-state at the end of the control horizon. However, if the control horizon is small, the strategy becomes infeasible. Krupa et al. (2019) enlarged this domain of attraction, especially for problems with a small control horizon, by applying parameterized periodic signals to track the desired reference in both inputs and outputs at the expense of increasing the number of decision variables.

An alternative approach is to design soft terminal equality constraints solely for integrating and unstable states with suitable slack variables. Santoro and Odloak (2012); Martins and Odloak (2016) developed stabilizing DMC-type (Dynamic Matrix Control-type) control strategies with zone control with these terminal ingredients. Their solution improves the feasibility of the control law because when disturbances excite the system, these slacks can tackle possible infeasibility issues. However, if unstable states are present, the stabilizing properties are only guaranteed when such slack variables are zeroed.

It is noteworthy that the challenge addressed is to minimize the conflict between enforcing both stabilizing properties and the feasibility of the optimization problem.

From this perspective, Santana et al. (2020) proposed two ingredients to enlarge the domain of attraction: (i) enforce solely non-stable states to be at an artificial steady-state at the end of the control horizon, through a terminal equality constraint, and (ii) soften the states bounds with slack variables, allowing to better accommodate unmeasured disturbances. The control law can simultaneously provide both stabilizing properties and feasibility of the optimization problem, even for a small control horizon. It is proposed here to design an MPC strategy with zone control, including the ingredients mentioned above, to enlarge the domain of attraction, suitable to track targets defined by an RTO layer. The optimization problem includes an artificial steady-state, output targets, and slacks as additional decision variables.

This work is organized as follows. Section 2 presents the proposed MPC strategy with zone control and optimizing targets, presenting its stabilizing properties, as well as ingredients to enlarge the domain of attraction. Section 3 presents a case study that explores the characteristics of the controller. Finally, Section 4 offers some concluding remarks.

2. CONTROL DESIGN

Consider a system described by the following linear model description:

$$\hat{\boldsymbol{x}}(j+1) = \hat{\boldsymbol{A}} \cdot \hat{\boldsymbol{x}}(j) + \hat{\boldsymbol{B}} \cdot \boldsymbol{u}(j), \tag{1}$$

where $\hat{\boldsymbol{x}}(j) \in \mathbb{R}^{(n\hat{x}\times 1)}$ is the state vector at time step j, $\boldsymbol{u}(j) \in \mathbb{R}^{(nu\times 1)}$ is the input vector, $\hat{\boldsymbol{A}} \in \mathbb{R}^{(n\hat{x}\times n\hat{x})}$ is the state matrix, and $\hat{\boldsymbol{B}} \in \mathbb{R}^{(n\hat{x}\times nu)}$ is the input matrix. Equation (1) can be converted into the velocity form (González et al., 2008), in order to design an offset free control law, by considering $\begin{bmatrix}\hat{\boldsymbol{x}}(j)\\ \boldsymbol{u}(j-1)\end{bmatrix} \in \mathbb{R}^{(n\hat{x}+nu\times 1)}$ as an augmented state vector:

$$\boldsymbol{x}(j+1) = \boldsymbol{A} \cdot \boldsymbol{x}(j) + \boldsymbol{B} \cdot \Delta\boldsymbol{u}(j), \tag{2}$$

$$\boldsymbol{y}(j) = \boldsymbol{C} \cdot \boldsymbol{x}(j), \tag{3}$$

where $\boldsymbol{x}(j) \in \mathbb{R}^{(nx\times 1)}$ is the augmented state vector at time step j, being $nx = n\hat{x} + nu$, $\Delta\boldsymbol{u}(j) \in \mathbb{R}^{(nu\times 1)}$ is the vector of input increments, $\boldsymbol{y}(j) \in \mathbb{R}^{ny\times 1}$ is the output vector, $\boldsymbol{A} = \begin{bmatrix}\hat{\boldsymbol{A}} & \hat{\boldsymbol{B}}\\ \boldsymbol{0} & \boldsymbol{I}\end{bmatrix} \in \mathbb{R}^{(nx\times nx)}$ is the state matrix, $\boldsymbol{B} = \begin{bmatrix}\hat{\boldsymbol{B}}\\ \boldsymbol{I}\end{bmatrix} \in \mathbb{R}^{(nx\times nu)}$ the input matrix, and $\boldsymbol{C} = \begin{bmatrix}\hat{\boldsymbol{C}} & \boldsymbol{0}\end{bmatrix} \in \mathbb{R}^{(ny\times nx)}$ the output matrix. $\hat{\boldsymbol{C}}$ is the output matrix related to (1).

The Jordan decomposition of the state-space model is applied to classify states in stable and non-stable, i.e. integrating or unstable modes (with or without multiplicities) by using $\boldsymbol{z} = \boldsymbol{W} \cdot \boldsymbol{x}$:

$$\boldsymbol{z}(j+1) = \begin{bmatrix}\boldsymbol{J}_\mathrm{s} & \boldsymbol{0}\\ \boldsymbol{0} & \boldsymbol{J}_\mathrm{ns}\end{bmatrix} \cdot \boldsymbol{z}(j) + \boldsymbol{W} \cdot \boldsymbol{B} \cdot \Delta\boldsymbol{u}(j), \tag{4}$$

$$\begin{bmatrix}\boldsymbol{J}_\mathrm{s} & \boldsymbol{0}\\ \boldsymbol{0} & \boldsymbol{J}_\mathrm{ns}\end{bmatrix} = \boldsymbol{W} \cdot \boldsymbol{A} \cdot \boldsymbol{V}, \tag{5}$$

where $\boldsymbol{V}$ is the generalized eigenvector, $\boldsymbol{J}_\mathrm{s}$ is the Jordan block associated with stable states, $\boldsymbol{J}_\mathrm{ns}$ is the Jordan block associated with non-stable states. Finally, the submatrices related to stable states, $\boldsymbol{W}_\mathrm{s}$, and non-stable states, $\boldsymbol{W}_\mathrm{ns}$, can be obtained from $\boldsymbol{W}$.

Assuming that there is an RTO layer that defines input targets, $\boldsymbol{u}_\mathrm{des}$, to be achieved by the control layer. Then, the zone tracking oriented MPC strategy is formulated in order to accommodate such targets, complying with operational zones, and unmeasured disturbances, namely:

Problem P0

$$\min_{\boldsymbol{x}_\mathrm{s},\Delta\boldsymbol{u}_k,\boldsymbol{\delta}_k,\boldsymbol{y}_\mathrm{t}} V_k = \sum_{j=0}^{N-1}\left\{\|\boldsymbol{x}(j)-\boldsymbol{x}_\mathrm{s}\|^2_{\boldsymbol{Q}_x} + \|\Delta\boldsymbol{u}(j)\|^2_{\boldsymbol{R}}\right\} + \\ + \|\boldsymbol{x}(N)-\boldsymbol{x}_\mathrm{s}\|^2_{\widetilde{\boldsymbol{Q}}_x} + \|\boldsymbol{u}_\mathrm{s}-\boldsymbol{u}_\mathrm{des}\|^2_{\boldsymbol{Q}_u} + \\ + \|\boldsymbol{y}_\mathrm{s}-\boldsymbol{y}_\mathrm{t}\|^2_{\boldsymbol{Q}_y} + \|\boldsymbol{\delta}_k\|^2_{\boldsymbol{S}} \tag{6}$$

subject to (2), (3) and:

$$\boldsymbol{x}(j=0) = \boldsymbol{x}(k), \tag{7}$$

$$\boldsymbol{x}(j) \in \mathcal{Z}_\mathrm{s},\ j=0,\ldots,N+k_2, \tag{8}$$

$$\Delta\boldsymbol{u}(j) \in \Delta\mathcal{U},\ j=0,\ldots,N-1, \tag{9}$$

$$\boldsymbol{y}_\mathrm{t} \in \mathcal{Z}_\mathrm{t}, \tag{10}$$

$$\boldsymbol{x}_\mathrm{s} \in \mathcal{X}_\mathrm{ss}, \tag{11}$$

$$\boldsymbol{W}_\mathrm{ns} \cdot (\boldsymbol{x}(N) - \boldsymbol{x}_\mathrm{s}) = \boldsymbol{0}, \tag{12}$$

where $\boldsymbol{Q}_x \in \mathbb{R}^{(nx\times nx)}$, $\boldsymbol{Q}_y \in \mathbb{R}^{(ny\times ny)}$, $\boldsymbol{Q}_u \in \mathbb{R}^{(nu\times nu)}$ are assumed to be positive semi-defined tuning matrices, while $\boldsymbol{R} \in \mathbb{R}^{(nu\times nu)}$, and $\boldsymbol{S} \in \mathbb{R}^{(n\hat{x}\times n\hat{x})}$ are positive definite tuning matrices. $\Delta\mathcal{U}$, $\mathcal{Z}_\mathrm{s}$, $\mathcal{Z}_\mathrm{t}$ are compact-convex sets related to bound constraints on input increments, states, and output trajectory, respectively:

$$\Delta\mathcal{U} = \{\Delta\boldsymbol{u} \in \mathbb{R}^{nu} \,|\, \Delta\boldsymbol{u}_\mathrm{min} \le \Delta\boldsymbol{u} \le \Delta\boldsymbol{u}_\mathrm{max}\}, \tag{13}$$

$$\mathcal{Z}_\mathrm{s} = \left\{\boldsymbol{x} \in \mathbb{R}^{nx} \,\middle|\, \begin{bmatrix}\hat{\boldsymbol{x}}_\mathrm{min}\\ \boldsymbol{u}_\mathrm{min}\end{bmatrix} \le \begin{bmatrix}\hat{\boldsymbol{x}}+\boldsymbol{\delta}_k\\ \boldsymbol{u}\end{bmatrix} \le \begin{bmatrix}\hat{\boldsymbol{x}}_\mathrm{max}\\ \boldsymbol{u}_\mathrm{max}\end{bmatrix}\right\}, \tag{14}$$

$$\mathcal{Z}_\mathrm{t} = \{\boldsymbol{y}_\mathrm{t} \in \mathbb{R}^{ny} \,|\, \boldsymbol{y}_\mathrm{min} \le \boldsymbol{y}_\mathrm{t} \le \boldsymbol{y}_\mathrm{max}\}. \tag{15}$$

$\boldsymbol{x}_\mathrm{s}$ is an artificial equilibrium point enforced by $\mathcal{X}_\mathrm{ss}$:

$$\mathcal{X}_\mathrm{ss} = \{\boldsymbol{x}_\mathrm{s} \in \mathcal{Z}_\mathrm{s} \,|\, (\boldsymbol{I}-\boldsymbol{A}) \cdot \boldsymbol{x}_\mathrm{s} = \boldsymbol{0}\}, \tag{16}$$

and can be expressed by $\begin{bmatrix}\hat{\boldsymbol{x}}_s^\top & \boldsymbol{u}_\mathrm{s}^\top\end{bmatrix}^\top$. Moreover, the output at this equilibrium point, $\boldsymbol{y}_\mathrm{s}$, is evaluated with $\boldsymbol{C} \cdot \boldsymbol{x}_\mathrm{s}$.

The slack variable, $\boldsymbol{\delta}_k$, is applied to soften the bounds on the state constraints and provide additional degrees of freedom for the controller to mitigate disturbances that excite the process. In this sense, $\boldsymbol{S}$ must be orders of magnitude higher than the other tuning matrices (Santana et al., 2020). Additionally, to comply with physical constraints of the system, one can include bound constraints to limit the slack variables in **Problem P0**.

Constraint (7) is such that $\boldsymbol{x}(0)$ is the initial condition of Problem P0, taken as the measured states at time step k. k_2 is a scalar to increase the prediction horizon in (8), aiming at ensuring the feasibility of this constraint on the infinite horizon, by imposing (8) up to time $N+k_2$ (Santana et al., 2020). Its value can be estimated from the steps described by Rawlings and Muske (1993).

The terminal cost weight, $\widetilde{\boldsymbol{Q}}_x$, is given by:

$$\widetilde{\boldsymbol{Q}}_x = \boldsymbol{W}_\mathrm{s}^\top \cdot \overline{\boldsymbol{Q}}_x \cdot \boldsymbol{W}_\mathrm{s}, \tag{17}$$

where $\overline{\boldsymbol{Q}}_x$ is the solution of the Lyapunov equation:

$$\overline{\boldsymbol{Q}}_x = \boldsymbol{V}_\mathrm{s}^\top \cdot \boldsymbol{Q}_x \cdot \boldsymbol{V}_\mathrm{s} + \boldsymbol{J}_s^\top \cdot \overline{\boldsymbol{Q}}_x \cdot \boldsymbol{J}_s, \tag{18}$$

and $\boldsymbol{V}_{\mathrm{s}}$ is the generalized eigenvector related to stable states obtained from (5).

It is noteworthy that in order to provide degrees of freedom to the controller, the output trajectory $\boldsymbol{y}_{\mathrm{t}}$ is a decision variable of the control problem that must be kept inside the operational zones (10). In this sense, the proposed controller aims to drive the process system toward the desired zone while maintaining the inputs as close as possible to the desired input targets, $\boldsymbol{u}_{\mathrm{des}}$.

Remark 1. Problem P0 combines two major ingredients presented by Santana et al. (2020) to enlarge the domain of attraction, allowing accommodation of disturbances. The first element is imposing terminal equality constraints solely on non-stable states (unstable and integrating states), which permanently enlarge the domain of attraction. The second element comprises the usage of slack variables to soften the bounds on the original states, $\hat{\boldsymbol{x}}$, enlarging the domain of attraction solely when it is needed.

2.1 Stability of the closed-loop system

Theorem 1 asserts that Problem P0 is nominally stable. In this sense, if the initial condition at time step k, $\boldsymbol{x}(0)$, belongs to the domain of attraction of the optimization problem, the controller maintains the system within such a domain and drives it to the reachable steady-state asymptotically.

Theorem 1. Consider a stabilizable ($\boldsymbol{A}$, $\boldsymbol{B}$) pair with n_{ns} non-stable poles and $N \geq (1+n_{\mathrm{ns}})/nu$. If the solution to Problem P0 is feasible at time step k, with appropriate k_2 to ensure the feasibility of the states bounds over the infinite horizon, then it will remain feasible at successive time steps. Thus, the successive solutions drive the closed-loop system asymptotically to a steady-state where the cost function V_k reaches its lowest achievable value.

Proof. The proof of this theorem builds on the concepts of recursive feasibility and convergence (Santana et al., 2020). Consider that $\left[\Delta \boldsymbol{u}_k^{*,\top} \;\; \boldsymbol{x}_{\mathrm{s}}^{*,\top} \;\; \boldsymbol{\delta}_k^{*,\top} \;\; \boldsymbol{y}_{\mathrm{t}}^{*,\top}\right]^{\top}$ is a feasible solution to Problem P0 at time step k, given any $\boldsymbol{x}(0)$ that belongs to its domain of attraction. The optimal cost function at this time step is:

$$\begin{aligned} V_k^* = \sum_{j=0}^{N-1} \left\{ \|\boldsymbol{x}(j) - \boldsymbol{x}_{\mathrm{s}}^*\|^2_{\boldsymbol{Q}_x} + \|\Delta \boldsymbol{u}^*(j)\|^2_{\boldsymbol{R}} \right\} + \\ + \|\boldsymbol{x}(N) - \boldsymbol{x}_{\mathrm{s}}^*\|^2_{\widetilde{\boldsymbol{Q}}_x} + \|\boldsymbol{u}_{\mathrm{s}}^* - \boldsymbol{u}_{\mathrm{des}}\|^2_{\boldsymbol{Q}_u} + \\ + \|\boldsymbol{C}\cdot\boldsymbol{x}_{\mathrm{s}}^* - \boldsymbol{y}_{\mathrm{t}}\|^2_{\boldsymbol{Q}_y} + \|\boldsymbol{\delta}_k^*\|^2_{\boldsymbol{S}}. \end{aligned} \tag{19}$$

Moving to time step $k+1$, it is shown that the solution inherited from time step k, $\left[\Delta \widetilde{\boldsymbol{u}}_{k+1}^{\top} \;\; \boldsymbol{x}_{\mathrm{s}}^{*,\top} \;\; \boldsymbol{\delta}_k^{*,\top} \;\; \boldsymbol{y}_{\mathrm{t}}^{*,\top}\right]^{\top}$, where $\Delta \widetilde{\boldsymbol{u}}_{k+1}^{\top} = \left[\Delta \boldsymbol{u}^{\top}(1), \; \ldots, \Delta \boldsymbol{u}^{\top}(N-1), \boldsymbol{0}^{\top}\right]^{\top}$ remains feasible. Firstly, the bound constraints (8) to (10) are satisfied by the inherited solution, as well as (11). Then, take the terminal equality constraint (12) at time step k:

$$\begin{aligned} \boldsymbol{W}_{\mathrm{ns}} \cdot (\boldsymbol{x}(N) - \boldsymbol{x}_{\mathrm{s}}^*) = \boldsymbol{0}, \\ \boldsymbol{W}_{\mathrm{ns}} \cdot \left(\boldsymbol{A}^N \cdot \boldsymbol{x}(0) + \boldsymbol{\Theta}_{\boldsymbol{N}} \cdot \Delta \boldsymbol{u}_k^* - \boldsymbol{x}_{\mathrm{s}}^* \right) = \boldsymbol{0}, \\ \boldsymbol{z}_{\mathrm{ns}}(N) = \boldsymbol{W}_{\mathrm{ns}} \cdot \boldsymbol{x}_{\mathrm{s}}^*, \end{aligned} \tag{20}$$

where $\boldsymbol{\Theta}_{\boldsymbol{N}}$ is $\left[\boldsymbol{A}^{N-1}\cdot\boldsymbol{B}, \cdots, \boldsymbol{B}\right]$. Therefore, the non-stable states, $\boldsymbol{z}_{\mathrm{ns}}(N)$, are at the artificial steady-state. Moving to the next time step, $k+1$, (12) gives:

$$\begin{aligned} \boldsymbol{W}_{\mathrm{ns}} \cdot \left(\boldsymbol{A}^N \cdot \boldsymbol{x}(1) + \boldsymbol{\Theta}_{\boldsymbol{N}} \cdot \Delta \widetilde{\boldsymbol{u}}_{k+1} - \boldsymbol{x}_{\mathrm{s}}^* \right) = \boldsymbol{0}, \\ \boldsymbol{W}_{\mathrm{ns}} \cdot \left(\boldsymbol{A} \cdot \left(\boldsymbol{A}^{\boldsymbol{N}} \cdot \boldsymbol{x}(0) + \boldsymbol{\Theta}_{\boldsymbol{N}} \cdot \Delta \boldsymbol{u}_k^* \right) - \boldsymbol{x}_{\mathrm{s}}^* \right) = \boldsymbol{0}, \\ \boldsymbol{J}_{\mathrm{ns}} \cdot \boldsymbol{z}_{\mathrm{ns}}(N) = \boldsymbol{W}_{\mathrm{ns}} \cdot \boldsymbol{x}_{\mathrm{s}}^*, \end{aligned} \tag{21}$$

as $\boldsymbol{z}_{\mathrm{ns}}(N)$ is at an equilibrium point, (20), then $\boldsymbol{z}_{\mathrm{ns}}(N) = \boldsymbol{J}_{\mathrm{ns}} \cdot \boldsymbol{z}_{\mathrm{ns}}(N)$, resulting in (21) to be equivalent to (20). Therefore, the inherited solution satisfies (12), and Problem P0 is recursively feasible.

Taking the difference of V_k^* and the cost function applying the inherited solution, $\widetilde{V}_{k+1}$, one has:

$$V_k^* - \widetilde{V}_{k+1} = \|\boldsymbol{x}(0) - \boldsymbol{x}_{\mathrm{s}}^*\|^2_{\boldsymbol{Q}_x} + \|\Delta \boldsymbol{u}(0)\|^2_{\boldsymbol{R}}. \tag{22}$$

Given that $\boldsymbol{Q}$ is assumed to be positive semi-definite, while $\boldsymbol{R}$ is assumed positive-definite, V_k^* must be greater or equal to $\widetilde{V}_{k+1}$. Moreover, since the inherited solution is only a feasible solution at time step $k+1$, and the cost function is convex, one can conclude that $V_{k+1}^* \leq \widetilde{V}_{k+1} \leq V_k^*$. This demonstrates that the cost function can never increase along with its time evolution, being a monotonically decreasing function, i.e. a Lyapunov-like function, resulting in an asymptotically convergent control law. □

Remark 2. Assuming that the closed-loop system reaches the steady-state, $\boldsymbol{x}_{\mathrm{s}}$, and provided that the cost function is a Lyapunov-like function, the minimum value for V_k is:

$$V_\infty = \|\boldsymbol{u}_{\mathrm{s}}^* - \boldsymbol{u}_{\mathrm{des}}\|^2_{\boldsymbol{Q}_u} + \|\boldsymbol{C}\cdot\boldsymbol{x}_{\mathrm{s}}^* - \boldsymbol{y}_{\mathrm{t}}\|^2_{\boldsymbol{Q}_y}, \tag{23}$$

i.e. a weighted sum between the distances of the controlled variables and outputs at the artificial steady-state from the desired input target, $\boldsymbol{u}_{\mathrm{des}}$, and the evaluated output target. In this sense, the weighting matrices $\boldsymbol{Q}_u$, $\boldsymbol{Q}_y$ defines the priority of attending the targets defined by the RTO layer or some operational conditions, respectively. If the input target is reachable and corresponds to the outputs inside the zone, then V_∞ is zero.

Remark 3. It is noteworthy that if the RTO layer defines an unreachable input target in conflict with the operational zone ($\boldsymbol{y}_{\min}$,$\boldsymbol{y}_{\max}$), it only affects the performance of the closed-loop system, without jeopardizing its feasibility, even in the presence of disturbances. Additionally, from Remark 2, one can conclude that the matrices $\boldsymbol{Q}_u$, $\boldsymbol{Q}_y$ define which aspect must be prioritized.

3. CASE STUDY

The case study addresses a Continuous Stirred Tank Reactor (CSTR) processing A→B, which must be controlled in the neighborhood of an unstable equilibrium point. The dimensionless model of the system is borrowed from Nagrath et al. (2002):

$$\frac{dy_1}{d\tau} = u_1 \cdot (1 - y_1) - 0.072 \cdot y_1 \cdot \kappa, \tag{24}$$

$$\frac{dy_2}{d\tau} = u_1 \cdot (-y_2) - 0.3 \cdot (y_2 - y_3) + 0.0576 \cdot y_1 \cdot \kappa, \tag{25}$$

$$\frac{dy_3}{d\tau} = \frac{u_2 \cdot (-1 - y_3)}{0.1} + \frac{0.3 \cdot (y_2 - y_3)}{0.05}, \tag{26}$$

$$\kappa = \exp\left(\frac{y_2}{1 + y_2/20}\right), \tag{27}$$

where τ is the dimensionless time, y_1 is the reactant A concentration, y_2 is the reactor temperature, y_3 is the cooling jacket temperature, u_1 is the feed flow rate of reactor and u_2 is the feed flow rate of the cooling fluid in the jacket. The unstable equilibrium point of interest is: 0.6364 ($y_{1_{ss}}$), 1.9146 ($y_{2_{ss}}$), -0.4823 ($y_{3_{ss}}$), 0.7232 ($u_{1_{ss}}$) and 2.7779 ($u_{2_{ss}}$). It is used a sampling time of 0.05 τ, and through linearization the following discrete state-space model is obtained (Santana et al., 2020):

$$\hat{\boldsymbol{x}}(j+1) = \begin{bmatrix} 9.44 \cdot 10^{-1} & -1.08 \cdot 10^{-2} & -4.99 \cdot 10^{-5} \\ 1.64 \cdot 10^{-1} & 1.04 \cdot 10^{0} & 7.41 \cdot 10^{-3} \\ 1.51 \cdot 10^{-2} & 1.48 \cdot 10^{-1} & 1.85 \cdot 10^{-1} \end{bmatrix} \cdot \hat{\boldsymbol{x}}(j) + \\ + \begin{bmatrix} 1.82 \cdot 10^{-2} & 4.85 \cdot 10^{-6} \\ -9.60 \cdot 10^{-2} & -1.20 \cdot 10^{-3} \\ -8.81 \cdot 10^{-3} & -1.25 \cdot 10^{-1} \end{bmatrix} \cdot \boldsymbol{u}(j) \tag{28}$$

$$\boldsymbol{y}(j) = \begin{bmatrix} 1 & 0 & 0 \\ 0 & 1 & 0 \\ 0 & 0 & 1 \end{bmatrix} \cdot \hat{\boldsymbol{x}}(j). \tag{29}$$

The controller parameters are: $\boldsymbol{Q} = \text{diag}([1.\ 1.\ 0.5\ 0.1\ 0.1])$, $\boldsymbol{R} = \text{diag}([2\ 2])$, $\boldsymbol{S} = \text{diag}\left(\left[10^2\ 10^2\ 10^2\right]\right)$, $\boldsymbol{Q}_y = \text{diag}([4\ 4\ 4])$, and $\boldsymbol{Q}_u = \text{diag}([1\ 1\ 1])$. The control horizon is $N = 2$, which is the minimum value defined by Theorem 1, since $\boldsymbol{A}$ has two integrating states and one unstable state. It must be emphasized that the slack weights are orders of magnitude higher than the other tuning weights. In this case study, it turns to be sufficient to define k_2 as zero.

In the simulation scenario, the system starts from the operating condition $[0.25\ -1.3\ -1.2]^\top$, which is outside the bounds on states (perturbed state). This forces the control law to use the $\boldsymbol{\delta}_k$ to ensure the feasibility of the optimization problem. Tables 1 and 2 describe the bound constraints, output zones and the input targets. Additionally, from 130 τ to 140 τ a persistent disturbance of -0.1 in the reactant concentration, y_1, excites the system.

Table 1. Bounds on states, inputs, inputs increments and slack variables.

$\hat{\boldsymbol{x}}^\top_{\max}$	$[0.2\ 2.0\ 1.0]$
$\hat{\boldsymbol{x}}^\top_{\min}$	$[-0.2\ -1.0\ -1.0]$
$\boldsymbol{u}^\top_{\max}$	$[4.0\ 6.0]$
$\boldsymbol{u}^\top_{\min}$	$[-0.5\ -1.]$
$\Delta\boldsymbol{u}^\top_{\max}$	$[0.25\ 0.5]$
$\boldsymbol{\delta}_{\max}$	$40\% \cdot \hat{\boldsymbol{x}}_{\max}$
$\boldsymbol{\delta}_{\min}$	$40\% \cdot \hat{\boldsymbol{x}}_{\min}$

Table 2. Zone definitions and targets on input variables. From 50 τ to 180 τ it is only indicated the changes between scenarios.

τ	$\boldsymbol{y}^\top_{\min}$	$\boldsymbol{y}^\top_{\max}$	$\boldsymbol{u}^\top_{\text{des}}$
0 to 49	$[-0.2\ -1.0\ -1.0]$	$[0.2\ 2.0\ 1.0]$	$[0.0\ 1.0]$
50 to 99	$[-0.2\ 0.0\ -1.0]$	$[0.0\ 2.0\ 1.0]$	$[-0.1\ 2.0]$
100 to 180	$[-0.2\ 1.0\ -1.0]$	$[-0.15\ 2.0\ 1.0]$	$[0.1\ 0.5]$

Figure 1 depicts that the control law can track the target imposed to inputs, $\boldsymbol{u}_{\text{des}}$, while maintaining the outputs inside their operational zones (Figure 2). It is noteworthy that some targets are unreachable for the controller, but it does not affect its feasibility, as stated by Remark 3.

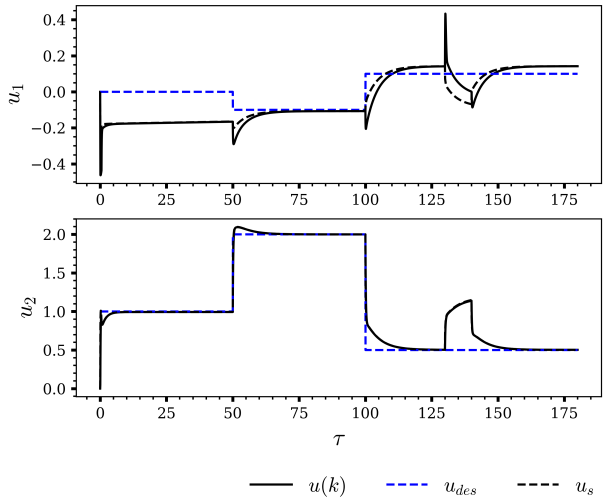

Figure 1. Input of the system.

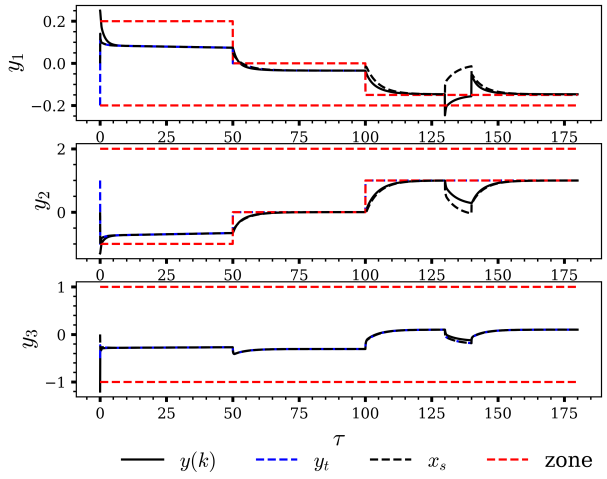

Figure 2. Outputs of the system.

One of the key ingredients of this strategy is to apply slack variables to soften the bound constraints on states (14). Figure 3 indicates that the controller only used such variables when the system was excited by disturbances that drove the states to outside their bounds, as asserted by Remark 1. In fact, the slack variables are non-zero between $[0,\ 0.5]$ τ, and $[130.05,\ 130.07]$ τ.

The effect of the slack variables in the domain of attraction is more evident in Figures 4 and 5. It is important to highlight that the domain of attraction is a polyhedral region $\mathcal{S}_N \subseteq \mathcal{Z}_s$ such that for all $\boldsymbol{x} \in \mathcal{S}_N$, **Problem P0** is feasible, i.e. this is a set of initial states $\boldsymbol{x}(0)$ that can be admissibly steered to the desired output zone in N steps. Such figures explicit the domain of attraction from the time when a disturbance enters into the system until the time when the slacks are zeroed.

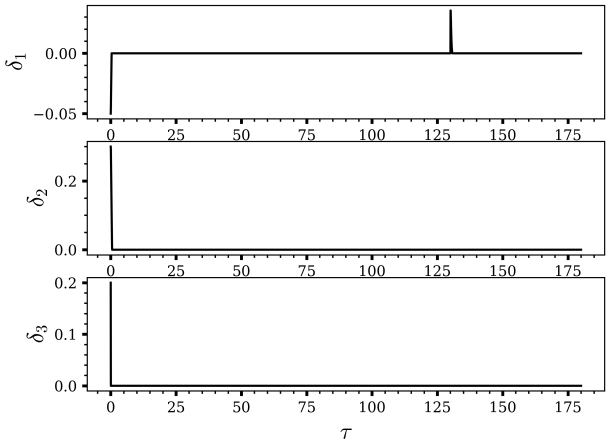

Figure 3. Slack variables of the system.

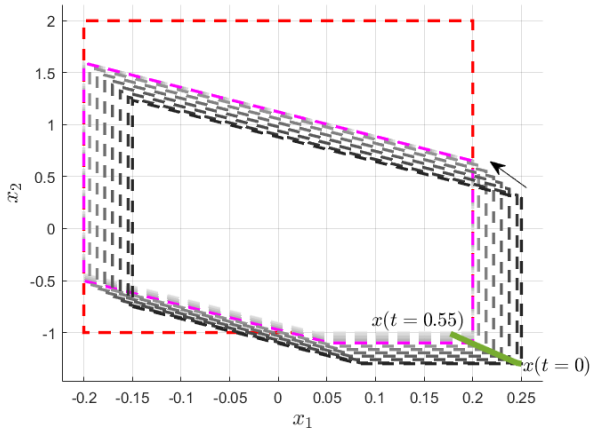

Figure 4. Domain of attraction of the proposed controller from the initial condition (black polyhedron) to the time 0.55 τ (lighter gray polyhedron). The magenta polyhedron represents the domain of attraction when the slack is zeroed. The control zone is represented in red. The system trajectory at the aforementioned time period is depicted in green.

Figure 4 depicts a shift in the domain of attraction (dashed black lines) to comply with the initial condition outside the bound constraints of states. Figure 5 depicts such a shift accommodating the disturbance that excites the process at 130 τ and drives the process to outside its states' bounds. Therefore, one can conclude that the slack variables enlarge the domain of attraction when necessary to avoid infeasibility issues. Furthermore, Figures 2 and 5 depict that when the disturbance excites the system, from $t = 130\ \tau$ to $t = 140\ \tau$, the control law can not fully comply with the defined zone, i.e. it drives the system toward a region where a steady-state exists (blue polyhedron) but outside the defined output zone (red polyhedron), without affecting its feasibility.

The abrupt change presented in the system trajectory in Figure 5 occurs at 140 τ due to the disturbance that affected y_1. However, since this happened inside the domain of attraction, the slack variables remained zeroed, Figure 3, consequently the domain of attraction is not

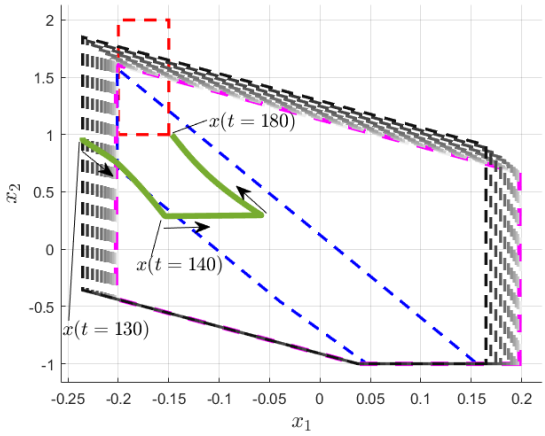

Figure 5. Domain of attraction of the proposed controller from the time 130 τ (black polyhedron) to the end of the simulation (lighter gray polyhedron). The magenta polyhedron represents the domain of attraction when the slack is zeroed. The control zone is represented in red. The blue polyhedron represents the region where there is an artificial steady-state, $\boldsymbol{x}_s$. The system trajectory at the aforementioned time period is depicted in green.

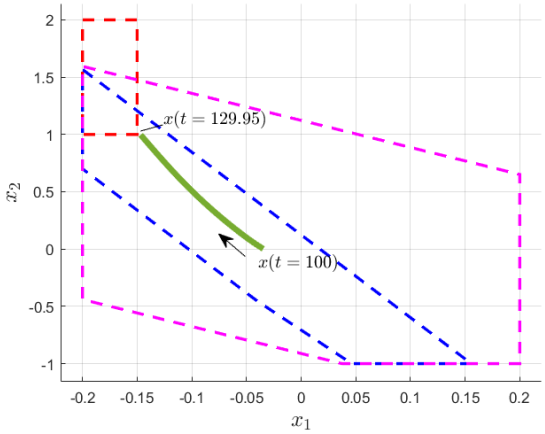

Figure 6. Domain of attraction (magenta polyhedron) of the proposed controller from the time 100 τ to the time 129.95 τ (the slack is zeroed). The control zone is represented in red. The blue polyhedron represents the region where there is an artificial steady-state, $\boldsymbol{x}_s$.The system trajectory at the aforementioned time period is depicted in green.

changed. Additionally, in such a scenario, the control law can drive the system toward the defined output zone.

Figure 6 depicts the domain of attraction of the smallest zone imposed to the controller when there is no disturbance, between 100 τ and 129 τ. Because the slack variables are zeroed, the domain of attraction remains unchanged. The trajectory is driven towards a region where there is an $\boldsymbol{x}_s$ (inside the blue polyhedron) and minimizes the distance from the defined output zone (red polyhedron).

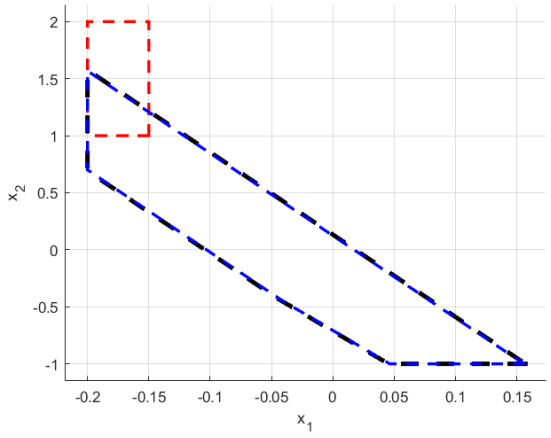

Figure 7. Domain of attraction (black polyhedron) of the control law when the terminal equality constraint (12) is set to be $\boldsymbol{x}(N) = \boldsymbol{x}_s$ and without slack variables. The desired zone is represented in red. The blue polyhedron represents the region where there is an artificial steady-state, $\boldsymbol{x}_s$.

In order to exemplify the effect of the terminal equality constraint (12), consider an alternative constraint in which $\boldsymbol{x}(N)$ must be at $\boldsymbol{x}_s$, as proposed by Ferramosca et al. (2009). Figure 7 depicts both the domain of attraction and the region where $\boldsymbol{x}_s$ exists. In this case study, the control horizon is small ($N = 2$) and such regions are almost the same. If we compare regions provided by figures 6 and 7, it is evident that by imposing solely non-stable states to be at the artificial equilibrium point, the domain of attraction of the proposed controller is therefore permanently enlarged, as asserted by Remark 1.

4. CONCLUSION

This work presented a zone tracking-oriented stabilizing MPC strategy, which aims to provide both feasibility and stabilizing properties, especially when the controller is subjected to unreachable targets produced by the RTO layer. Such properties are achieved by terminal equality constraints regarding non-stable states to be at an artificial steady-state that tracks the desired RTO targets. It is demonstrated that the control law guides the closed-loop system towards a steady-state that minimizes the distance between the RTO targets and the operational zones.

Another key aspect is to circumvent infeasible conditions provided by unmeasured disturbances. Then, suitable slack variables soften the bound constraints on states and can enlarge the domain of attraction when needed.

The case study exemplifies the effect of each ingredient in the closed-loop performance. It focuses especially on the permanent enlargement of the domain of attraction provided by the terminal equality constraint design and the temporary change in the domain of attraction provided by the slack variable.

ACKNOWLEDGMENTS

The authors thank the Brazilian research agencies Capes, CNPq and FAPESB.

REFERENCES

Ferramosca, A., Limon, D., Alvarado, I., Alamo, T., and Camacho, E. (2009). MPC for tracking with optimal closed-loop performance. *Automatica*, 45(8), 1975–1978.

Ferramosca, A., Limon, D., González, A., Odloak, D., and Camacho, E. (2010). MPC for tracking zone regions. *Journal of Process Control*, 20(4), 506–516. doi:10.1016/j.jprocont.2010.02.005.

González, A.H., Adam, E.J., and Marchetti, J.L. (2008). Conditions for offset elimination in state space receding horizon controllers: A tutorial analysis. *Chemical Engineering and Processing: Process Intensification*, 47(12), 2184–2194.

González, A.H. and Odloak, D. (2009). A stable MPC with zone control. *Journal of Process Control*, 19(1), 110–122. doi:10.1016/j.jprocont.2008.01.003.

Krishnamoorthy, D., Foss, B., and Skogestad, S. (2018). Steady-state real-time optimization using transient measurements. *Computers and Chemical Engineering*, 115, 34–45. doi:10.1016/j.compchemeng.2018.03.021. URL `https://doi.org/10.1016/j.compchemeng.2018.03.021`.

Krupa, P., Pereira, M., Limon, D., and Alamo, T. (2019). Single harmonic based Model Predictive Control for tracking. In *2019 IEEE 58th Conference on Decision and Control*. IEEE, Nice, France. doi:10.1109/CDC40024.2019.9029488.

Marchetti, A., Ferramosca, A., and González, A. (2014). Steady-state target optimization designs for integrating real-time optimization and model predictive control. *Journal of Process Control*, 24(1), 129–145. doi:10.1016/j.jprocont.2013.11.004.

Martins, M.A.F. and Odloak, D. (2016). A robustly stabilizing model predictive control strategy of stable and unstable processes. *Automatica*, 67, 132–143. doi:10.1016/j.automatica.2016.01.046.

Nagrath, D., Prasad, V., and Bequette, B. (2002). A model predictive formulation for control of open-loop unstable cascade systems. *Chemical Engineering Science*, 57(3), 365–378.

Rawlings, J.B. and Muske, K.R. (1993). The Stability of Constrained Receding Horizon Control. *IEEE Transactions on Automatic Control*, 38(10), 1512–1516.

Santana, D.D., Martins, M.A.F., and Santos, T.L.M. (2020). A stabilizing gradient-based economic MPC for unstable processes: toward the enlargement of the domain of attraction. In *Anais do Congresso Brasileiro de Automática 2020*. sbabra. doi:10.48011/asba.v2i1.1717.

Santoro, B.F. and Odloak, D. (2012). Closed-loop stable model predictive control of integrating systems with dead time. *Journal of Process Control*, 22(7), 1209–1218. doi:10.1016/j.jprocont.2012.05.005.

Santos, J.E.W., Trierweiler, J.O., and Farenzena, M. (2021). Model Update Based on Transient Measurements for Model Predictive Control and Hybrid Real-Time Optimization. *Industrial & Engineering Chemistry Research*, 60(7), 3056–3065. doi:10.1021/acs.iecr.1c00212.

Scattolini, R. (2009). Architectures for distributed and hierarchical Model Predictive Control - A review. *Journal of Process Control*, 19(5), 723–731. doi:10.1016/j.jprocont.2009.02.003.